Characteristic Modes Approach to Design Compact Superdirective Array With Enhanced Bandwidth

Hussein Jaafar, Sylvain Collardey, Ala Sharaiha

Characteristic Modes Approach to Design Compact Superdirective Array With Enhanced Bandwidth

Hussein Jaafar, Sylvain Collardey, and Ala Sharaiha, *Senior Member, IEEE*

***Abstract*—Superdirective arrays have become the key technique in enhancing the directivity of electrically small antennas. By forming an array of closely spaced unit elements, a high directivity can be achieved. Despite the high directivity, these arrays suffer from narrow bandwidth and low efficiency. In this paper, we present an approach to enhance the bandwidth of superdirective arrays using the network characteristic modes. The key step, is to use an internally loaded compact wideband unit element. The loads inside the unit element are used to manipulate the characteristic modes in order to optimize its impedance bandwidth. A two-element end-fire array is then formed. The modal coefficients of the characteristic fields are then optimized at multiple frequency point in order to radiate a maximal directivity in the end-fire direction. The best current excitation that can maintain a constant directivity as a function of frequency is then deduced. Finally a feeding network that can provide the desired excitation at the array ports is designed and integrated on the array system, where the $1dB$ directivity bandwidth is about 23% with D_{max} = $7.1dBi$. The antenna impedance bandwidth is equal to 15%.**

***Index Terms*—Superdirectivity, network characteristic modes, compact antennas, multiport antennas.**

I. Introduction

Compact antennas are physically limited in bandwidth, effciency and directivity [1]–[3]. As the size of the antenna reduces with respect to the wavelength, its efficiency and bandwidth will degrade dramatically and its radiation pattern approaches a quasi-omnidirectional form, leading to radiations in undesired directions. Nevertheless, the massive development in wireless communication systems, imposes the need for compact and directive antennas to be integrated in limited spaces of the wireless devices.

Superdirective array antennas can be an attractive technique in overcoming the omnidirectional radiation pattern of small antennas. By forming an array of closely spaced elements ($d < 0.25\lambda$) an extraordinary directivity called "superdirectivity" can be achieved [6]–[15]. Several works on superdirectivity focused on the upper directivity limits with respect to the antenna size. Uzkov [6] showed that the directivity of N closely spaced isotropic radiators can achieve N^2 if each element is properly excited in phase and magnitude. On the other hand, Harrington showed that the maximum directivity of an antenna enclosed in a sphere of raduis r can achieve $N^2 + 2N$ where $N = kr$ and k is the wave number [3].

In [8] Altshuler *et al* studied the superdirectivity of a two elemenent endfire array as a fuction of frequency. By optimizing the phase and magnitude of the two driven elements, it was shown that the array exhibits a superdirectivity for close spacing. Moreover, as the distance between the elements decreases ($d < 0.2\lambda$), their input resistance decreases to the point that the ohmic loss becomes significant. Therefore, the array suffered from low efficiency and narrow bandwidth. Later, Best *et al.* suggested using high impedance folded wire monopoles mounted on a large ground plane as unit elements in a two-element endfire array, in order to eleminate the effect of the ohmic loss at very close separation distances [9]. Despite the narrow impedance and directivity bandwidth, with an inter-element separation of 0.1λ the array achieved a peak directivity of $10.18dB$ and about 90% efficiency.

On the other hand, in order to avoid multiple excitation for array elements in fully driven configuration. Haskou *et al* proposed a simple approach to design compact parasitic loaded superedirective arrays [10]. In this technique, only one element is driven and the other parasitic elements are reactively loaded. The reactive loads are calculated from the active impedance in order to provide the optimal relative current magnitude and phase with respect to the driven element. Taking a narrow band half-loop ESA integrated on a PCB as a unit element, a two-element array was formed. A maximal directivity of $7.1dB$ was obtained in the endfire direction, which is almost equivalent to that of a fully driven configuration.However, the impedance and directivity bandwidths were limited to $1.7MHz$ (0.18%) and $2.1MHz$ (0.2%) respectively. Nevertheless, in [11] O'Donnell demonstrated that the choice of low Q antennas as unit elements can offer a higher directivity bandwidth.

To address the issue of narrow bandwidth in superdirective array, we present in this paper the design of wideband superdirective arrays based on internally loaded wideband small unit element. The design methodolgy is based on the theory of the network characteristic modes (NCM) [16]. Using the NCM optimization technique presented in [19], a wideband compact unit element is designed. This unit element is internally loaded with inductive loads. The inductive loads are used to manipulate the NCM's on the antenna in order to match it in a desired bandwidth. Furthermore, a two-element end-fire array is formed. The array exhibits a wide impedance bandwidth. In order to optimize the directivity in the endfire direction, the weighting coefficients of the characteristic fields are optimized

Manuscript received 13 April, 2017. This work is supported by the European Union through the European Regional Development Fund (ERDF), and by Ministry of Higher Education and Research, Brittany and Rennes Métropole, through the CPER Project SOPHIE / STIC & Ondes, and by the Direction Général de l'Armement (DGA). The authors are with IETR UMR CNRS 6164, Université de Rennes 1,35042 Rennes Cedex, France (e-mail: hussein.jaafar@univ-rennes1.fr)

at different frequency points in the bandwidth of operation using the method presented in [17], [18]. The performance of the arrays is then studied for a parasitic loaded case. However in order to achieve a wider directivity bandwidth, we propose the integration of a feed network on the array. This network provides the array elements with the proper phase and magnitude to maintain a relatively constant and high end-fire directivity over a wide bandwidth.

In section II, we first review the NCM theory and the different steps of the approach. In section III, we present the design of a wideband superdirective array, starting with an internally loaded wideband unit element. The superdirectivity of a two element end-fire array is then studied for both parasitic and fully driven cases. The NCM is then used to analyze the results and deduce the required excitation to maintain a wideband directivity in the end-fire direction. Then, the prototype of the wideband superdirective array with the integrated feeding network is given in section IV.

II. NCM and Design methodology

A. Network Characteristic Modes

The network characteristic modes is a numerical technique used to describe the eigen modes of a multiport network based on its impedance matrix [16]. The NCM formulation follows the same approach as the classical Characteristic Modes CMs [20]–[22], however the modes are extracted from the N-port Z-matrix rather than the MOM Z matrix. The design approach presented in this paper is based on the optimization of the NCM's in the unit element and then optimizing the excitation coefficients of the network characteristic fields in the array to maximize the directivity in a specific direction. For an N-port network the NCM's are obtained from the generalized eigenvalue problem:

$$[X_a]\bar{J}_n = \lambda_n[R_a]\bar{J}_n \tag{1}$$

$$\bar{J} = \sum_{n=1}^{N} \frac{\tilde{J}_n^* \bar{V}_{oc}(\omega)\bar{J}_n}{(1+j\lambda_n)(\tilde{J}_n^*[R_a]\bar{J}_n)} = \sum_{n=1}^{N} a_n \bar{J}_n \tag{2}$$

$$Y_{in}[input] = \sum_{n=1}^{N} \frac{\bar{J}_n[input]^2(1-j\lambda_n)}{(1+\lambda_n^2)(J_n^*[R_a]\bar{J}_n)} = \sum_{n=1}^{N} Y_n \tag{3}$$

where R_a and X_a are respectively the real and imaginary parts of the impedance matrix of an N-port antenna. $\bar{J}_n$ is the characteristic current vector at the defined ports and V_{oc} is the open circuit voltage vector . a_n is the modal weighting that shows the contribution of each mode in the overall radiation. Each characteristic current J_n radiates a characteristic field E_n. Consequently the total radiated field can also be expressed as a weighted summation of the characteristic fields:

$$E = \sum_{n=1}^{N} a_n E_n \tag{4}$$

B. Design Methodology

First step in the design process is to miniaturize and enlarge the bandwidth of the unit element based on the method used in [19],which combines the NCM with the Differential Evolution (DE) optimization algorithm [23]. Specific port locations are defined inside the unit element, and then reactive loads are used to manipulate the input admittance of the radiating NCMs such that the antenna is matched in a wide bandwidth. Starting form a wideband small antenna as a unit element, an N-element array is formed. Then at a specific frequency point, the modal weighting coefficients are optimized to maximize the directivity in a given direction using the DE algorithm [17], [18]. The total directivity at a specific angle (θ_0, ϕ_0) can be written as a function of the modal weighting coefficients:

$$D(\theta_0,\phi_0) = 4\pi \frac{|E_\theta(\theta_0,\phi_0)|^2 + |E_\phi(\theta_0,\phi_0)|^2}{\int_0^{2\pi}\int_0^{\pi}(|E_\theta(\theta,\phi)|^2 + |E_\phi(\theta,\phi)|^2) sin\theta d\theta d\phi} \tag{5}$$

given that:

$$E_\theta(\theta,\phi) = a_1 E_{1\theta}(\theta,\phi) + a_2 E_{2\theta}(\theta,\phi) + \cdots + a_N E_{N\theta}(\theta,\phi) \tag{6}$$

$$E_\phi(\theta,\phi) = a_1 E_{1\phi}(\theta,\phi) + a_2 E_{2\phi}(\theta,\phi) + \cdots + a_N E_{N\phi}(\theta,\phi) \tag{7}$$

where $[E_{1\theta}, \cdots, E_{N\theta}]$ are the characteristic far field components in θ direction and $[E_{1\phi}, \cdots, E_{N\phi}]$ are the characteristic far field components in ϕ direction. $[a_1, \cdots, a_N]$ are the modal weighting coefficients.

Choosing an appropriate objective function $F(a)$ is important to ensure the convergence of the algorithm to the desired goals. In this study the $F(a)$ is defined as:

$$F(\alpha) = w_1 \times D(\theta_0,\phi_0) + w_2 \times real(Z_{Li}) \tag{8}$$

where w_1 and w_2 are the weight factors that balance the contribution of each term in the cost function. w_2 varies depending on the array configuration, for a parasitic loaded configuration, $w_2 = 0.5$ while for a fully driven configuration $w_2 = 0$. The weighting factor w_2 is used to minimize (or eliminate) the real part of the loads Z_{Li} on the parasitic elements, in order to prevent the resistive losses in the antenna system. Z_{Li} is calculated using the following equation:

$$Z_{Li} = \frac{-[Z_a][I_{port}]_i}{[I_{port}]_i} \tag{9}$$

where Z_a is the $N \times N$ impedance matrix of the array and I_{port} is the port current that can be calculated from (2). It should be noted that this optimization is done for a single frequency point. Hence, in order to study the array directivity in a wideband, multiple optimization are done at different frequency point. The detailed steps of the design process are given below:

1. Define the unit element and use the NCM optimization to miniaturize it and optimize its bandwidth
2. Form an N-element array based on the unit element
3. Define the frequency band in which wide-band directivity is needed
4. Extract the N-port Z matrix of the array

5. At each frequency point

5*a*) Extract the characteristic currents using matlab

5*b*) Excite the array elements with the characteristic current vector to extract the corresponding characteristic field from the full wave simulation

5*c*) Input the characteristic fields in the optimization algorithm

6. For parasitic configuration

6*a*) Set $w_2 = 0.5$

6*b*) Extract the optimized parasitic load values at each frequency point

6*c*) Deduce the reactive load that can maintain a wideband directivity over the desired frequency

7. For fully driven configuration

7*a*) Set $w_2 = 0$

7*b*) Extract the optimized weighting coefficients at each frequency point.

7*c*) Calculate the corresponding current vector using (2) at each frequency point

7*d*) Deduce the best current magnitude and phase at the ports that can maintain a wideband directivity

7*e*) Design and optimize a feed network the can provide the desired amplitude and phase.

7*f*) Integrate the feeding network on the PCB of the array

In the next section the design of a two-element wideband superdirective array based on wideband unit element will be presented.

III. Wideband Superdirective Array

A. Unit Element

The unit element of the array is presented in Fig. 1. The antenna is an S-shaped monopole integrated on a PCB and mounted on a $0.76mm$ Rogers RT5880 substrate ($\epsilon_r = 2.2, tan\delta = 0.0009$). On the bottom side, a parasitic meander line is connected through a via to the ground plane. The inductive meander line reacts with the capacitive near field of the monopole, leading to a resonance at lower frequency. Using the bandwidth optimization methodology, the antenna is loaded at two positions with inductive loads $L_1 = 13nH$ and $L_2 = 28nH$. The overall dimensions are $(130mm \times 60mm)$, while the radiating element dimensions (antenna and parasitic meander line) are confined to $(13mm \times 60mm)$.

With the optimized inductive loads, the antenna is matched over a wide bandwidth $[0.85 - 1.05GHz]$ (Fig. 2a) which represents 20% relative to the central frequency, and exhibits an efficiency higher that 80% over the bandwidth (Fig. 2b). In this bandwidth, the antenna radiates a quasi-omnidirectional pattern with null along the x-axis (Fig. 3).

The next step is to form a compact superdirective array based on this wideband unit element, and to study the possibility to achieve a higher directivity bandwidth in both parasitic and driven cases.

B. Two-Element Endfire Array

After designing the internally loaded wideband unit element, a two element end-fire array is formed. The array geometry

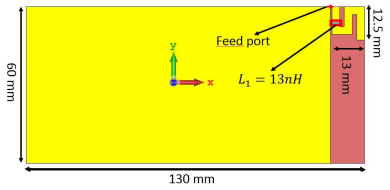

(a)

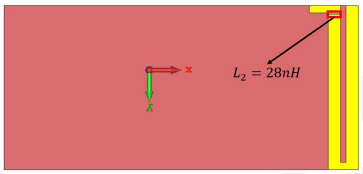

(b)

Fig. 1. Unit element. (a) Top view, (b) bottom view.

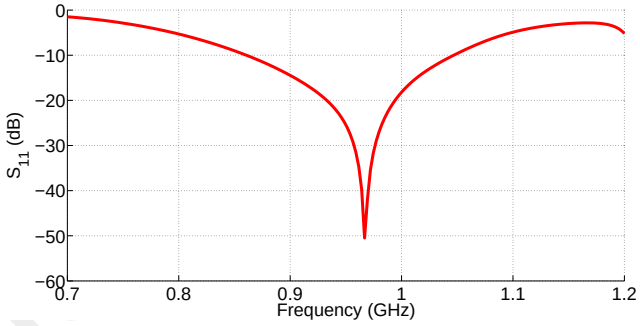

(a)

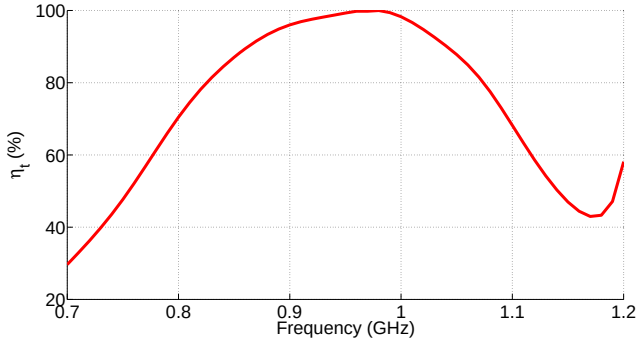

(b)

Fig. 2. Unit element. (a) Input reflection coefficient, (b) total efficiency.

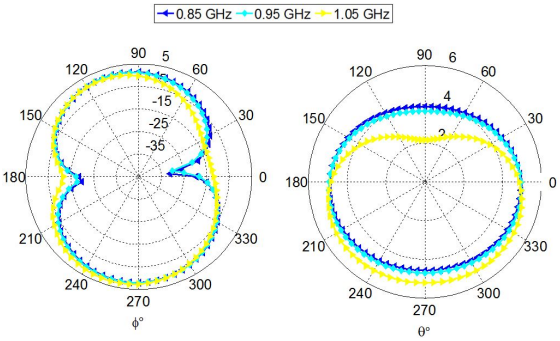

Fig. 3. 2-D total directivity radiation pattern of the unit element at different frequency points. Horizontal plane (left), vertical plane (right).

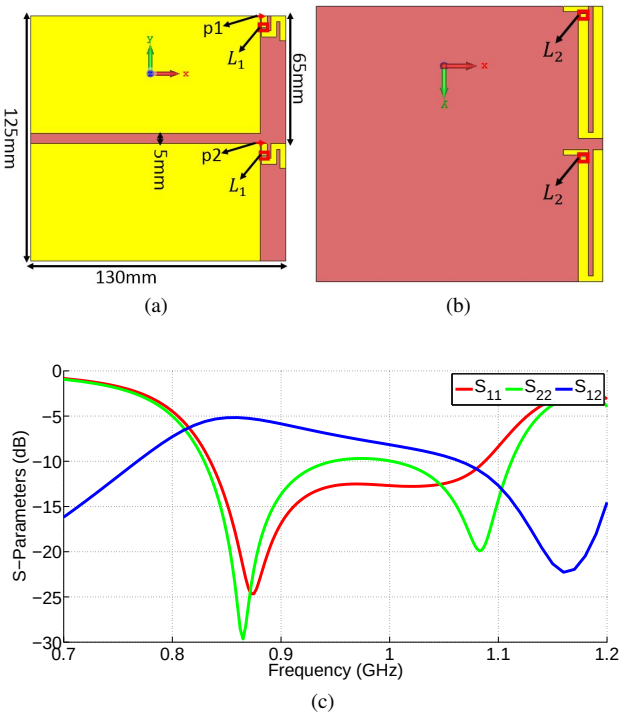

Fig. 4. Two element end-fire array. (a) Top view, (b) bottom view (c) S-parameters in dB.

and dimensions with respect to $\lambda = 348mm$ ($f = 0.86GHz$) are given in Fig.4. The inter-element separation is set to 0.18λ. Due to the dimensions of the ground plane of the unit elements, it is not possible to achieve lower separation distances. The S-parameters of the two-element array are given in Fig.4c. The mutual coupling of the array attains a peak value of $-5dB$ at about $0.85GHz$ after which it starts to decrease as the frequency increases. For a matching level of $S_{ii} < -10dB$, the array exhibits a wideband impedance matching $[0.83-1.11GHz]$ for port 1 and $[0.835-1.09GHz]$ for port 2 which represents 28.9% and 26.5% respectively with respect to the central frequency. Therefore an end-fire array with wideband impedance matching is formed. In the next step, the directivity of the array in parasitic configuration is optimized at different frequency points, to demonstrate the effect of using a wideband unit element on the directivity bandwidth.

C. Parasitic Configuration

In this section, the directivity of the array in a parasitic configuration is optimized . Port $p1$ is driven while port $p2$ is loaded. The optimization is done at different frequency points in the frequency band where the antenna is matched. As explained in the previous section, the objective function of (8) is used. Since the DE minimizes the objective function, $w1$ is set to -1 in order to maximize the directivity in the end-fire direction, where $\phi_0 = 270°$ and $\theta_0 = 90°$. In order to minimize the resistance of the parasitic load at the second port w_2 is set to 0.5 and $i = 2$. The optimization is initialized at $0.83GHz$. The impedance matrix of the array at $0.83GHz$ is given by:

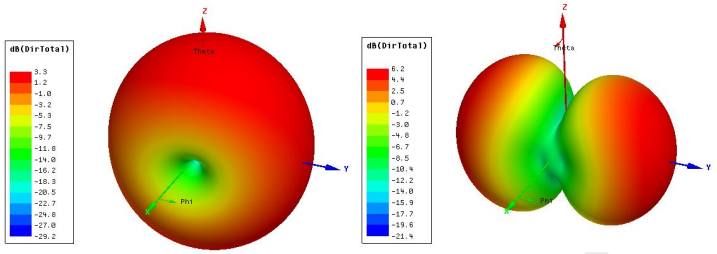

Fig. 5. Directivity of the network characteristic field at 0.83 GHz. (a) E_1, (b) E_2.

$$Z_a = \begin{bmatrix} 25.7 - 37.1i & 16.6 - 34.2i \\ 16.6 - 34.2i & 29.9 - 37.8i \end{bmatrix} \tag{10}$$

The two network characteristic currents are then calculated using (1):

$$I_1 = \begin{bmatrix} -0.99 \\ 1 \end{bmatrix}; I_2 = \begin{bmatrix} -1 \\ 0.65 \end{bmatrix} \tag{11}$$

The array ports are then excited by the characteristic currents I_1 and I_2 respectively using HFSS [24]. The 3D radiation pattern of the characteristic fields E_1 and E_2 are shown in Fig. 5. E_2 exhibits a bi-directional pattern ($D_{max} = 6.2dBi$) in the end-fire direction, while that of E_1 is more quasi-omnidirectional with a null along the x-axis ($D_{max} = 3.8dBi$).

The components of the characteristic fields are then imported in the optimization algorithm, in order to optimize the modal weighting coefficients a_1 and a_2, after which the corresponding parasitic load is calculated from Eqn. 9. The optimization yields an inductive parasitic load of value $3.6nH$ loaded at port $p2$. With this load the array achieves a peak end-fire directivity of $7dBi$ at $\phi = 270°$, a $5.5dBi$ FBR (Fig.7a) and a 98% radiation efficiency at $0.83MHz$. The array is matched in a wideband $[0.82 - 1.04GHz]$ (24%) (Fig. 7b). However, the $1dB$ directivity bandwidth is just limited to 7.1% ($[0.81 - 0.87GHz]$) (Fig. 6a). The degradation in the antenna directivity in the band beyond $0.87GHz$ can be explained by studying the normalized modal weighting coefficients α_1 and α_2 as a function of frequency (Fig. 6b). In the band where the antenna is directive, the directive mode 2 contributes more in the antenna radiation compared to mode 1, which results in an overall directive antenna. Yet, there is still a significant contribution from the first characteristic fields, that reacts with the directive field (E_2) resulting in maximal end-fire directivity. However, with the variation of the reactance of the passive parasitic load as a function of frequency, it becomes hard to establish a relatively stable excitation, that can maintain the dominance of the directive modes over a wideband, and hence maintaining a constant directivity.

Furthermore, the same study has been done at different frequency points. The results are summarized in Table. I. With the optimized parasitic loads, the array maintains a relatively constant peak directivity of $7dBi$ in the end-fire direction

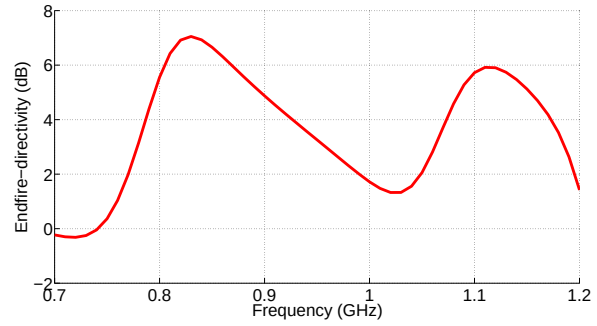

(a)

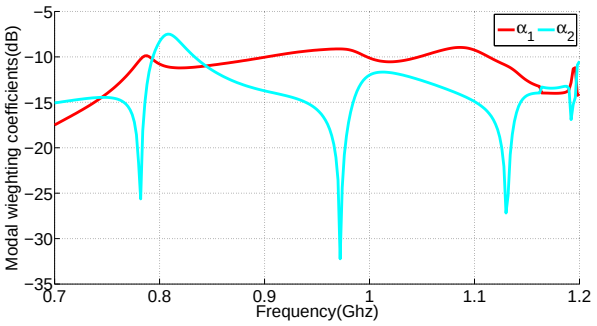

(b)

Fig. 6. (a) End-fire directivity (ϕ = 270°) as a function of frequency, (b) Normalized modal weighting coefficient.

TABLE I
OPTIMIZED PARASITIC LOAD VALUES AT DIFFERENT FREQUENCY POINTS

$f(GHz)$	$load$	$D(dB)$	$BW_{1dB}(\%)$	$\eta_r(\%)$	FBR
0.83	$3.6nH$	7	7.1	98	5.5
0.88	$10.94pF$	7	8.9	99	5.2
0.93	$3.2pF$	6.9	10.7	99	5.3
0.98	$1.3pF$	6.76	11.1	100	5.7
1.03	$0.9pF$	6.4	12.3	100	7.1

(ϕ = 270°) and a high radiation efficiency. On the other hand, the directivity bandwidth increases as the optimization frequency increases. The 2-D directivity radiation patterns of the parasitic loaded array at the optimization frequencies is given in Fig.8. For all the optimized parasitic loads, the arrays exhibits a relatively constant radiation pattern. Therefore, a wideband directivity can be achieved by providing the optimal reactance at the parasitic element. This reactance establishes the optimal excitation phase and magnitude to have a maximal directivity.

Fig. 9a shows the variation of the optimal parasitic reactance value as a function of frequency. The reactance (blue curve) exhibits a negative slope as a function of frequency which corresponds to a non-Foster load . With such load, a relatively constant directivity is maintained over the entire bandwidth of operation (green curve). From a modal point of view, loading the parasitic element with the non-Foster load, maintains the dominance of the second mode with respect to the first one (Fig. 9b), which provides the proper excitation in order to achieve a wideband directivity over the whole bandwidth.

Therefore, in order to maintain a wideband directivity as a function of frequency for a parasitic configuration, a non-

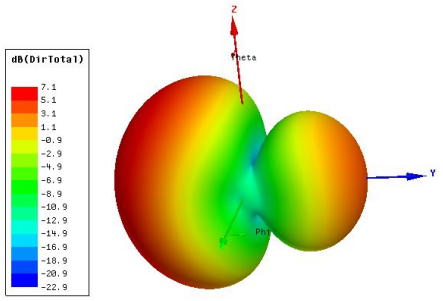

(a)

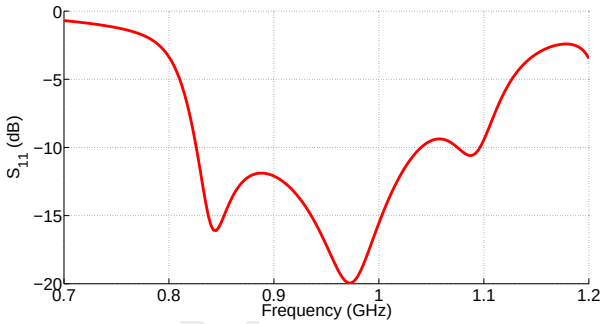

(b)

Fig. 7. End-fire parasitic array loaded with $3.6nH$ inductance. (a) Total directivity at $0.83GHz$, (b) input reflection coefficient.

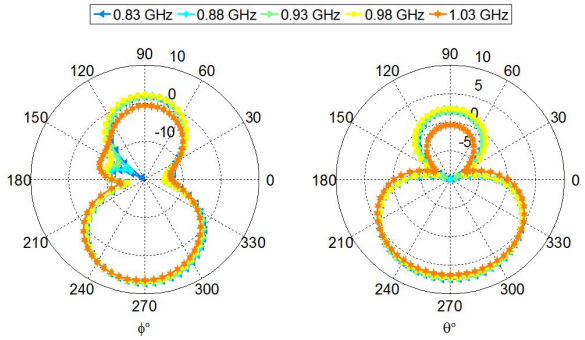

Fig. 8. 2-D total directivity radiation pattern. Horizontal plane (left), vertical plane (right).

foster load should be added at the second port $p2$. In order to avoid the complexity of non-foster circuit design, we present in the next section the design of a wideband superdirective array by integrating a feed network that provides the required excitation at the array ports to maintain a constant directivity.

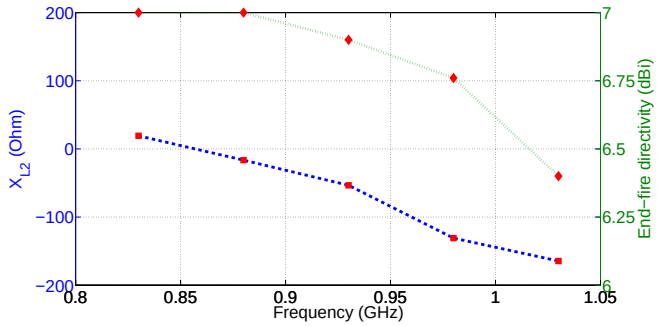

(a)

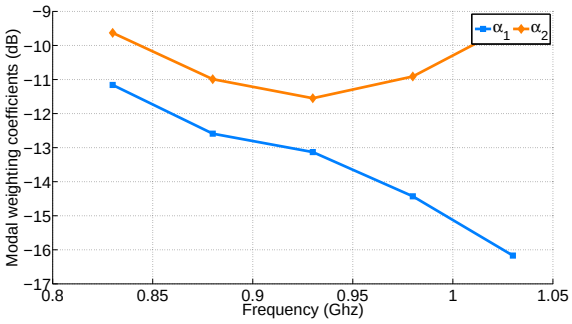

(b)

Fig. 9. Optimal parasitic loads. (a) Optimal parasitic reactance value the gives a maximal directivity, (b) Normalized modal weighting coefficient based on optimal reactive loads.

D. Fully Driven Configuration

In the case where both antennas are driven, the weighting factor w_2 is set to zero, since no parasitic loads are needed, while $w_1 = -1$. Similar to the previous section, the directivity optimization is carried at different frequencies. At each frequency point, modal weighting coefficients are optimized and the total current is extracted from (2). Fig. 10 shows the optimized relative current phases and magnitudes and their corresponding end-fire directivities at each frequency of optimization. With these excitation, the array attains a maximal directivity of $7.13dBi$ at $0.88GHz$ after which it slightly decreases to become $6.82dBi$ at $1.03GHz$. Therefore, if the array ports are fed with the optimized excitation at each frequency point, it is possible to have a wideband directivity over the whole band. By analyzing the relative current and phase magnitude, we find that a trade off can be made by providing a constant excitation at the ports while maintaining a relatively constant peak directivity. From Fig. 10a the relative current amplitude at the first four optimization points ranges slightly between 0.58 and 0.715 while it becomes 2.2 at $1.03GHz$. However, as the frequency becomes higher, the inter-element separation as a function of the wavelength increases, and the array becomes less sensitive the changes in the excitation amplitude or phase. Therefore, a current relative magnitude of 0.7 ($\frac{I_1}{I_2} = 0.7$) is chosen as the best compromise to feed the array ports.

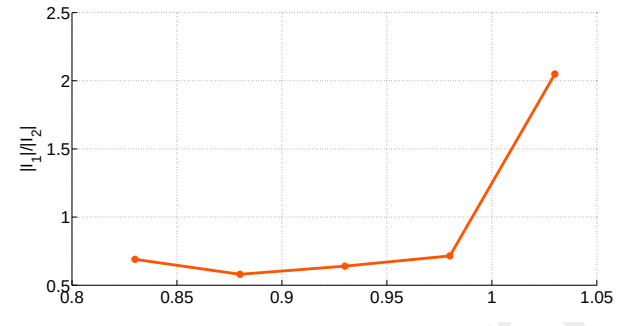

(a)

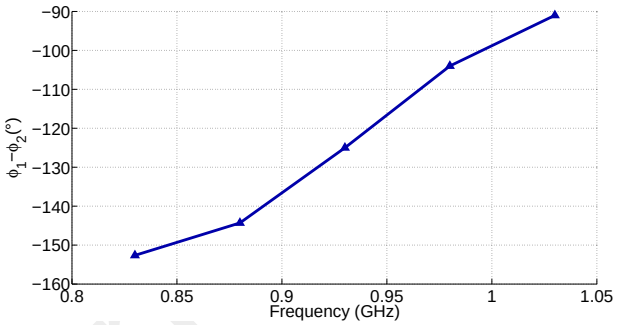

(b)

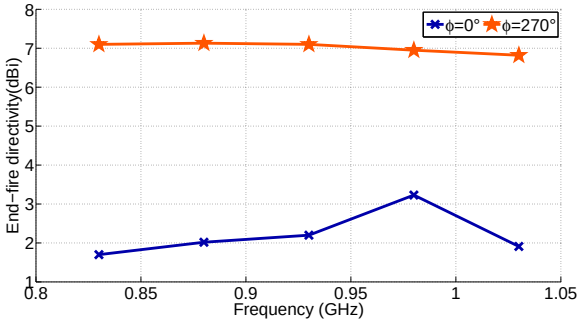

(c)

Fig. 10. Optimized current excitation at the array ports. (a) Magnitude, (b) phase, (c) end-fire directivity in the horizontal plane.

Nevertheless, in order to identify the best relative current phase at the array ports, the end-fire directivity behaviour of the array versus frequency was studied for three different currents . These excitations have a similar relative magnitude ($\frac{I_1}{I_2} = 0.7$), while different relative phase values were considered for each excitation ($\phi_1 - \phi_2 = -90°, -110°, -130°$). These values were chosen from the optimized relative phase values that are given in Fig.10b. Fig.11 shows the variation of the front ($\phi = 270°$) and back ($\phi = 270°$) end-fire directivities for the specified relative phases while maintaining a constant relative magnitude. For all the excitations, it is noticed that the directivity behaviour remains relatively unchanged beyond $1GHz$. This is due to the fact that the inter-element separation distance increases as the wavelength decreases and hence the array becomes less sensitive to phase changes.

The $-130°$ relative phase exhibits a stable directivity in the front direction with a peak value of $7.1dBi$ and is associated with an acceptable front-to-back ratio over the bandwidth un-

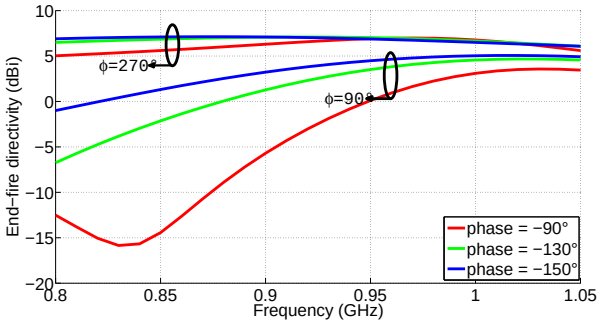

Fig. 11. End-fire directivity as a function of frequency for constant excitations.

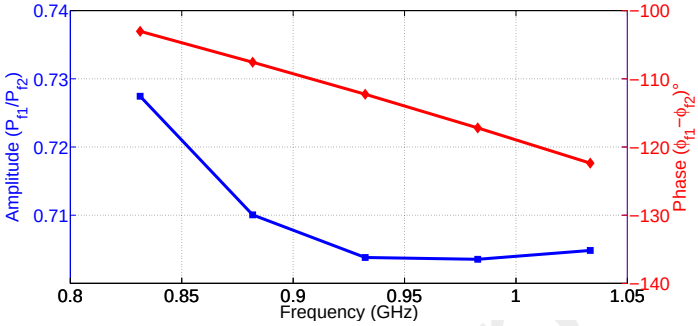

Fig. 12. Simulated performance of the feeding network.

der study. On the other hand, the front-to-back ratio is high for an excitation of relative phase which equals to $-90°$, however the directivity exhibits a $1.7dB$ drop in the bandwidth, where it achieves a maximal value of $7dBi$ at $0.95GHz$ and it drops down to $5.36dBi$ at $0.83GHz$. Moreover, the excitation with relative phase of $-150°$ exhibits the lowest front-to-back ratio over frequency while it maintains a relatively stable peak end-fire directivity. Therefore, a relative excitation of $\frac{I_1}{I_2} = 0.7e^{-j130^\circ}$ presents the best compromise in maintaining the directivity stability and an acceptable front-to-back ratio over a wide bandwidth.

With this excitation, the array achieves a peak directivity of $7.1dBi$ in the end-fire direction ($\phi = 270°$) at $0.92GHz$. The $1dB$ directivity drop bandwidth is more than 23% from $0.8GHz$ up to $1.05GHz$. Hence a feed network should be designed and well integrated on the array structure in order to provide the chosen relative phase and magnitude at the ports so that the directivity remains constant, while maintaining the impedance matching of the array.

E. Feeding Network Design

Before starting the design of the feed network, it is necessary to transform the desired current excitation into power excitations. The transformation into power excitation is given by:

$$P_n = I_n^2 Z_{active(n)} e^{-j4\pi(n-1)d} \tag{12}$$

P_n, I_n, and $Z_{active(n)}$ are respectively the power and current excitations, and the active impedance at the n^{th} port. d is the inter-element separation as a function of lambda. The relative power excitation corresponding to the chosen current excitation is $\frac{P_1}{P_2} = 0.75e^{-j130^\circ}$, where P_1 is the power delivered to port 1 and P_2 is the power delivered to port 2. Therefore the desired feed network should be formed of an unequal power divider cascaded with a phase shifter.

The parameters of the feeding network are optimized to provide the desired power excitations at its output, its behaviour in terms of delivered power and phase shift is shown in Fig. 12. The power ratio at the two ports is approximately stable over the desired bandwidth $0.7 < \frac{P_{f1}}{P_{f2}} < 0.74$, where P_{f1} and P_{f2} are the output powers of the feeding network delivered respectively to ports 1 and 2 of the array. Although the phase shift $(\phi_{f1} - \phi_{f2})$ is changing over the margin of change $(100° - 127°)$ between $(0.8 - 1.05GHz)$ it is still acceptable to maintain a high and relatively constant end-fire directivity. This variation will mainly affect the front to back ratio of the array as it was shown with the different relative excitations studied in Fig.11.

After finalizing the schematic design of the feed network, the next step is integrating it on the array structure without affecting the overall performance.

F. Integration of the Feeding network

Although it might seem a straight forward process, careful attention should be taken while integrating the feeding network in order not to perturb the currents on the array structure and deteriorate its performance. Especially that there is a gap between the ground planes of the two elements. A transmission line passing below this gap, might significantly alter the radiations of the array. Consequently, the characteristic modes analysis (CMA) is used to provide us with guidelines on defining the placement and the geometry of the feeding network.

The surface current distribution of the first two characteristic modes at 950 MHz is given in Fig.13 and their modal significance in the band if interest is shown in Fig.14. By examining this current distribution we conclude that in order to minimize the effect of the feeding network on the behaviour of the modes, some constraints on its topology must be set. The feeding network topology should be as far as possible from the points where the modal current distribution is high, which are mainly the upper edges of the ground planes. In addition the transmission line passing under the gap should also be from the farthest possible from the upper edges.

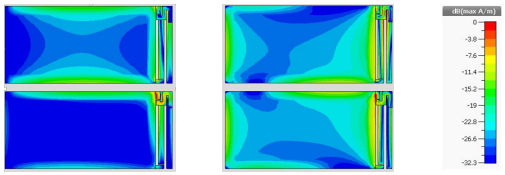

(a) (b) (c)

Fig. 13. Modal surface current distribution. (a) Mode 1, (b) mode 2, (c) scale, (d) modal significance of the first two modes.

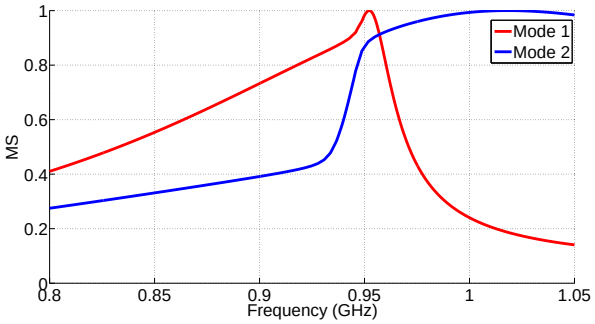

Fig. 14. Modal significance of the first two modes in the original array.

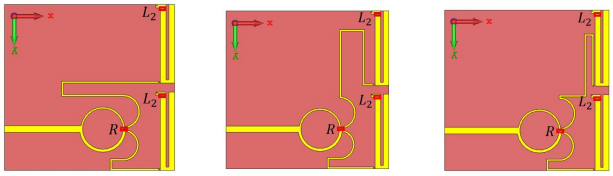

(a) (b) (c)

Fig. 15. Different topologies of integrated feeding network. (a) Case 1, (b) case 2, (c) case 3.

To verify this observation, three topologies of the integrated feeding network are considered for comparison (Fig.15). The feeding network of case 1 presents the topology that mostly agrees with the constraints that were set based on CMA where the line under the gap is as far as possible from the upper edges and it passes under the part where the current distribution is low for both modes. In addition, the transmission lines are not interfering with the upper edge current. On the other hand, in the topology of case 2 the line under the gap is closer to the upper edge and the transmission line of the phase shifter is interfering with the edge currents of the lower antenna. A more extreme case is shown in (Fig.15c) where the transmission lines are concentrated under the upper edge of the lower antenna. The modal significance of these three cases are compared with respect to the array without integrated feed (Fig.16). As expected the feeding network of case 1 presents the best modal performance, in which the effect on the first two original array modes is minimal. For case 2, the effect of is more visible in mode 1 where its resonance shifts about $40MHz$ while mode 2 remains in general unchanged, except in the upper part of the band where it becomes less significant. Case 3 presents the maximal effect in perturbing the modes especially mode 1 whose resonance is shifted from $0.95GHz$ to $0.82GHz$, in addition to its effect on mode 2 whose modal significance drops in the upper part of the band.

The consequence of perturbing the modal behaviour of the array is visualized in its radiation and impedance characteristics. Fig. 17 shows the front and backwards end-fire directivity of the array with the three integrated feeds compared to the case where the electromagnetic effect of the feeding network is not taken into account (ideal feed). As expected, the end-fire directivity of case 1 exhibits the best performance among the other cases. The directivity at ϕ = 270° is stable in the band with a 23% bandwidth, and a maximal value of $6.1dBi$

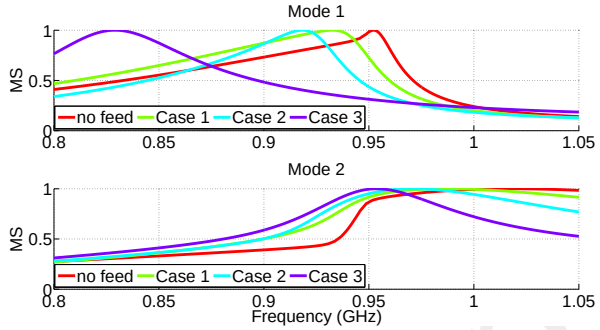

Fig. 16. Modal Significance of the original array and the three feeding topologies.

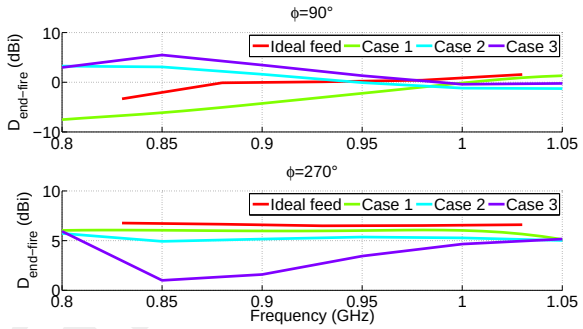

Fig. 17. Endfire directivity versus frequency of the array with the three integrated feeding networks compared to the ideal current excitations.

which is just $0.4dBi$ less than the ideal case. Moreover, the backwards radiations of case 1 are lower than that of the ideal case. However, for case 2, the directivity drops to $5dBi$ and the backwards radiations are high, on the other hand the maximal end-fire directivity for case 3 is switched to ϕ = 90° which however exhibits a narrowband.

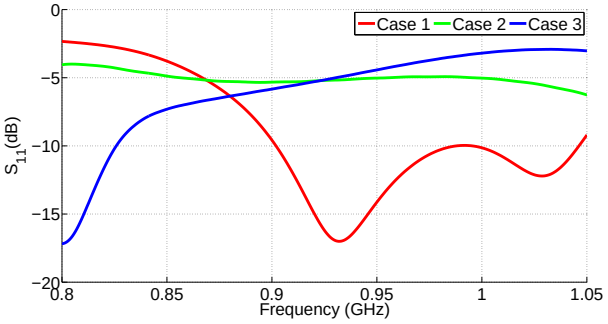

Fig. 18. Input reflection coefficients for the cases of the integrated feeding networks.

Fig.18 shows the input reflection coefficient of the above three cases. Case 1 exhibits the best impedance performance where the array is matched in 15% relative bandwidth $[0.9 - 1.04GHz]$, while case 2 is mismatched in the whole band and case 3 is matched in the lower part of the band. Therefore, using the characteristic modes analysis it was possible to define a specified feeding network topology with the minimal

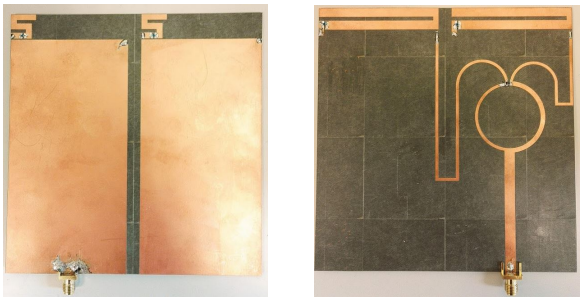

(a) (b)

Fig. 20. Prototype of the array. (a) Top view, (b) bottom view.

effect on the original modes supported by the array structure in order to maintain a stable directivity which is similar to that provided when the ideal feeding network is connected to the array.

After analyzing the performance of the different feeding topologies, it is obvious that case 1 presents the best performance in maintaining the desired array performance.

The geometry details of the final array design are given in Fig.19. The lumped components connected to the array are represented in colored boxes where $R = 111\Omega$ (decoupling resistor), $L_1 = 13nH$ and $L_2 = 28nH$. The dimensions associated to the final geometry are given in TableII.

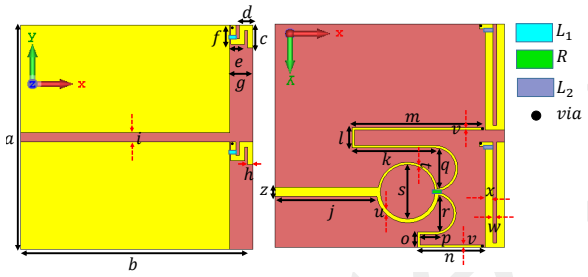

Fig. 19. Detailed geometry of the final design.

TABLE II
DIMENSIONS OF THE FINAL ANTENNA DESIGN IN mm

$a = 125$	$b = 130$	$c = 12.5$	$d = 7.75$	$e = 7.75$
$f = 10.7$	$g = 13$	$h = 2.3$	$i = 5$	$j = 59$
$k = 47$	$l = 11.5$	$m = 74.5$	$n = 37.4$	$o = 9$
$p = 12$	$q = 23$	$r = 21$	$s = 31$	$t = 1.33$
$u = 2.21$	$v = 1.37$	$w = 1.95$	$x = 4.5$	$z = 5$

IV. EXPERIMENTAL VALIDATION

The prototype of Fig. 20 was measured. Measurement results are shown in Fig. 21, which agree with the simulation results. The fabricated antenna is matched in a 12% bandwidth $[0.92 - 1.03GHz]$ which is a bit narrower than the simulation results (Fig.21a).

In addition, the array has a wideband directivity over the whole bandwidth with a peak directivity of $6.1dBi$. The measured end-fire directivity exhibits a relatively constant peak value in the direction $\phi = 270°$ over the entire bandwidth. On the other hand, the measured backwards radiations ($\phi = 90°$) are lower than the simulated ones. Fig. 21c shows the comparison between the measured and simulated total efficiency of the array. The array efficiency was measured using the wheeler cap method. The measurements are also in good agreement with the simulation. the measured prototype is efficient in the operating bandwidth, with a peak efficiency of 78% at $0.97GHz$.

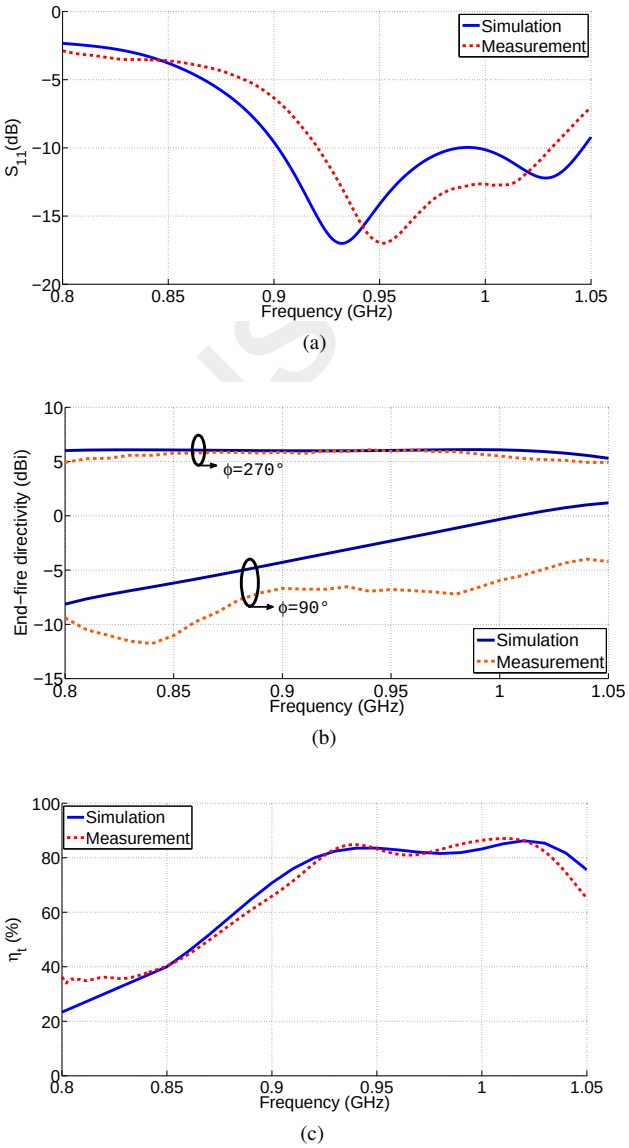

Fig. 21. Measurement results of the fabricated antenna. (a)Input reflection coefficient, (b) end-fire directivity in the front ($\phi = 270°$) and backwards ($\phi = 90°$) directions, (c) total efficiency.

The measured co and cross polar radiation patterns of the array in the E and H-planes at different frequency points are given in Fig.22. The measured array maintains a relatively stable radiation pattern with a cross-polarization discrimination of about $10dBi$ in the main lob direction $\phi = 270°$, $\theta = 90°$. The co-to-cross polar realized gain in the main lobe direction is given in Fig.23. The array exhibits a stable realized gain of $5dBi$ the bandwidth where it is matched $[0.92 - 1.03GHz]$ while the cross-polarization level is lower than $-5dBi$ in this band.

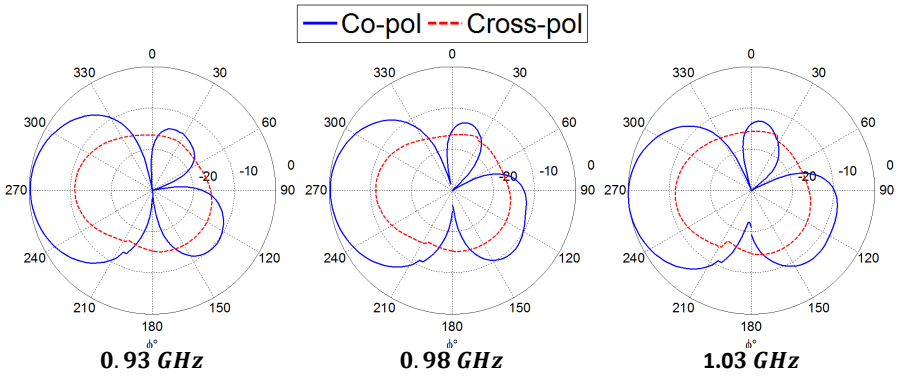

(a)

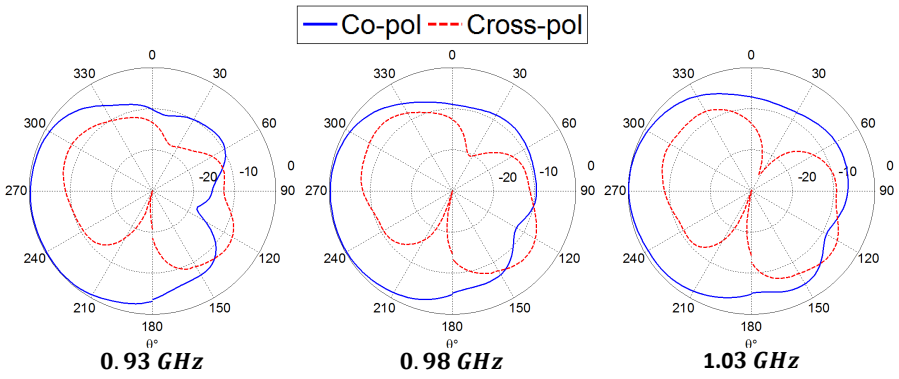

(b)

Fig. 22. Measured radiation pattern at different frequency points in the operating bandwidth. (a) E-plane (xy plane), (b) H-plane (yz plane).

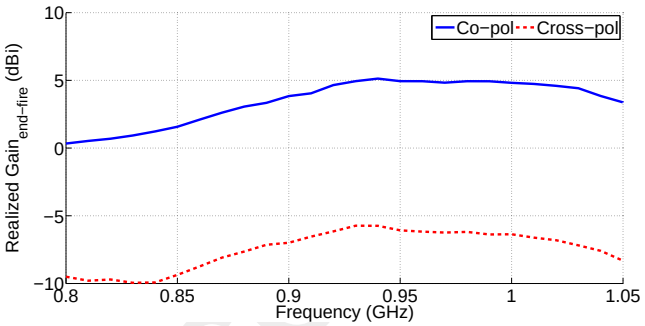

Fig. 23. Measured co- to cross-polarization gain.

V. Conclusion

In this paper we presented the design of a wideband superdirective array. First an internally loaded wideband unit element is designed using NCM optimization. Inductive loads are placed at two positions inside the unit element. These loads are capable of controlling the modes inside the antenna in order to match it in a 20% band. A two-element end-fire array is then formed based on this element. The array exhibits a wideband behaviour in terms of impedance. In order to study the possibility of obtaining a wideband directivity, using a wideband unit element, two configurations are considered. Starting with a parasitic configuration, the directivity bandwidth becomes limited since the modal weighting coefficient of the second mode (directive mode) becomes lower than that of the first mode (quasi-omnidirectional mode) apart from the optimization frequency. However, with non-Foster load, the dominance of the second mode can be maintained over the desired frequency range and hence wideband directivity is achieved. Nevertheless, in order to avoid the complexity of non-foster circuit, we propose the integration of a feeding network on the array structure. By feeding the array elements with the desired excitation, and by properly integrating the feed network on the array, it was possible to achieve a wideband superdirectivity. The measured array attains a peak directivity of $6.1dBi$ with a directivity bandwidth of 23% in which the array is matched over 12%.The measurements results are in good agreement with the simulation in which the array exhibits a similar directivity bandwidth with a peak D_{max} = $6.1dBi$ and impedance bandwidth 15%. Compared to the designs presented in literature [8]–[14], this array presents a significantly enhanced performance in terms a directivity and impedance bandwidth.

This technique can be applied on arrays with more elements. Having more elements in the array will generate higher order characteristic modes which offers higher degrees of freedom in optimizing the directivity and hence the array becomes more directive. However, despite achieving a higher directivity, some limitation might be associated. Mismatches might arise due to the increased coupling between the elements which

implies the need to re-optimize the internal loads inside the array, in addition to a decrease in the directivity bandwidth. Therefore, with more elements, the design process of a wide-band superdiective array becomes more complex and more parameters should be taken into account in the optimization process.

REFERENCES

[1] L. J. Chu, "Physical limitations of omni-directional antennas," *J. Appl.Phys.*, vol. 19, no. 12, pp. 11631175, Dec. 1948.

[2] J.H. Wheeler, "Fundamental Limitations of Small Antennas," *Proceedings of IRE*, vol. 35, December 1947, pp. 1479-1484.

[3] R. F. Harrington, "On the gain and bandwidth of directional antennas," *IRE Trans. Antennas Propag.*, vol. 6, no.3,pp. 219-225, Jul. 1958.

[4] Q. Liu, J. Shen, H. Liu, Y. Wu, M. Su and Y. Liu, "Low-Cost Compact Circularly Polarized Directional Antenna for Universal UHF RFID Handheld Reader Applications," in *IEEE Antennas and Wireless Propagation Letters,* vol. 14, pp. 1326-1329, 2015.

[5] M. M. M. Ali and A. R. Sebak, "Compact UWB high gain fermi taper slot antenna for future 5G communication systems," *2016 17th International Symposium on Antenna Technology and Applied Electromagnetics (ANTEM),* Montreal, QC, 2016, pp. 1-2.

[6] I. Uzkov, "An approach to the problem of optimum directive antennae design," *C. R. (Dokladey) Acad. Sci. lURSS,*,vol. 53, no. 1, pp. 35-38,1946.

[7] E. N. Gilbert and S. P.Morgan "Optimum design of directive antenna arrays subjet to random variations," *Bell Syst. Tech. J.,*,vol. 34, pp. 637-663, May 1955.

[8] E. E. Altshuler, T. H. O'Donnell, A. D. Yaghjian and S. R. Best, "A monopole superdirective array," *IEEE Transactions on Antennas and Propagation*, vol. 53, no. 8, pp. 26532661, Aug. 2005.

[9] S. R. Best, E. E. Altshuler, A. D. Yaghjian, J. M. McGinthy and T. H. O'Donnell, "An Impedance-Matched 2-Element Superdirective Array," *IEEE Antennas and Wireless Propagation Letters,* , vol. 7, pp. 302-305, 2008.

[10] A. Haskou, A. Sharaiha and S. Collardey,"Design of Small Parasitic Loaded Superdirective End-Fire Antenna Arrays," *IEEE Transactions on Antennas and Propagation*, vol. 63, no.12, pp. 54565464, Dec,2015.

[11] T. H. O'Donnell and A. D. Yaghjian, "Electrically small superdirective arrays using parasitic elements," *2006 IEEE Antennas and Propagation Society International Symposium,* Albuquerque, NM, 2006, pp. 3111-3114.

[12] T. H. O'Donnell, A. D. Yaghjian and E. E. Altshuler,"Frequency optimization of parasitic superdirective two element arrays," *2007 IEEE Antennas and Propagation Society International Symposium,* ,Honolulu, HI, 2007, pp. 3932-3935.

[13] A. Haskou, A. Sharaiha and S. Collardey,"Integrating Superdirective Electrically Small Antenna Arrays in PCBs," in *IEEE Antennas and Wireless Propagation Letters,* vol. 15, pp. 24-27, 2016.

[14] A. Clemente, M. Pigeon, L. Rudant and C. Delaveaud, "Design of a Super Directive Four-Element Compact Antenna Array Using Spherical Wave Expansion," in *IEEE Transactions on Antennas and Propagation,* vol. 63, no. 11, pp. 4715-4722, Nov. 2015.

[15] H. Jaafar, A. Sharaiha and S. Collardey, "Design of a wideband superdirective endfire antenna array using characteristic modes optimization," *2017 XXXIInd General Assembly and Scientific Symposium of the International Union of Radio Science (URSI GASS)*, Montreal, QC, 2017, pp. 1-4.

[16] J. Mautz and R. Harrington, "Modal analysis of loaded N-port scatterers," *IEEE Transactions on Antennas and Propagation,* vol. 21, no. 2, pp. 188-199, Mar 1973.

[17] Y. Chen and C. F. Wang, "Synthesis of Reactively Controlled Antenna Arrays Using Characteristic Modes and DE Algorithm," *in IEEE Antennas and Wireless Propagation Letters*,vol. 11, no. , pp. 385-388, 2012.

[18] Y. Chen and C. F. Wang, "Electrically loaded Yagi-Uda antenna optimization using characteristic modes and differential evolution," *J. Electromagn. Waves Appl.*, vol. 26, pp. 1018-1028, 2012.

[19] H. Jaafar, S. Collardey and A. Sharaiha,"Optimized Manipulation of the Network Characteristic Modes for Wideband Small Antenna Matching," *IEEE Transactions on Antennas and Propagation,* , vol. PP, no. 99, pp. 1-1.

[20] R. Harrington and J. Mautz, "Theory of characteristic modes for conducting bodies," in IEEE Transactions on Antennas and Propagation, vol. 19, no. 5, pp. 622-628, Sep 1971.

[21] R. Harrington and J. Mautz, "Computation of characteristic modes for conducting bodies," in IEEE Transactions on Antennas and Propagation, vol. 19, no. 5, pp. 629-639, Sep 1971.

[22] A. Yee and R. Garbacz, "Self- and mutual-admittances of wire antennas in terms of characteristic modes," *IEEE Transactions on Antennas and Propagation*, vol. 21, no. 6, pp. 868-871, Nov 1973.

[23] R. Storn and K. Price, "Minimizing the real functions of the ICEC96 contest by differential evolution", *Proc. IEEE Conf. Evol. Computat.*, Nagoya, 1996, pp. 842-844.

[24] ANSYS HFSS, Pittsburg, PA, USA.